DOI: 10.1002/adma.200600647

Three-Dimensional Biochemical and Biomechanical Patterning of Hydrogels for Guiding Cell Behavior**

By *Mariah S. Hahn*, *Jordan S. Miller*, and *Jennifer L. West**

The ability to tailor the biochemical and biomechanical properties of 3D materials at the microscale is important for a range of biotechnology applications, including the engineering of complex tissues, the development of biosensors, the elucidation of cell–cell and cell–material interactions, and the guidance of cellular differentiation.[1,2] To this end, techniques have emerged for the fabrication of 3D microcontrolled materials, including conventional photolithographic patterning,[3,4] electrochemical deposition,[5] 3D printing,[6] and soft-lithographic approaches.[7–10] To create internally complex 3D materials, these methods are repeated in a layer-by-layer fashion until a scaffold of the desired dimensionality is achieved. However, an alternate approach to the fabrication of internally complex 3D scaffolds, that is, the patterning of bioactivity into preformed materials of the desired final dimensions, has not been similarly examined.[11–13] Here, we develop a new paradigm for generating 3D microcontrolled materials using two-photon absorption (TPA) photolithography to pattern bioactivity into existing photoactive materials. We demonstrate the ability to spatially tailor material biomechanical and biochemical properties at the microscale and to create freeform 3D patterns and gradients. Furthermore, to illustrate the power of this approach for guiding cell behavior, proteolytically degradable hydrogels were patterned in 3D with the cell adhesive peptide arginine–glycine–aspartic acid–serine (RGDS), and cells were shown to invade and migrate into only the RGDS-containing regions.

In the present study, we first establish the feasibility of patterning bioactive features into optically transparent, photoactive materials using an adaptation of conventional photolithography, that is, single-photon absorption (SPA) photolithography. Although, as previously mentioned, SPA photolithography has been used to create topographical microstructures on surfaces,[3] it has not, to the best of our knowledge, been developed for the internal modification of preformed materials. We show that SPA photolithography allows for rapid and inexpensive biochemical and biomechanical patterning of existing photoactive materials in three dimensions. However, pattern complexity is limited to features of axially uniform cross section, since light passes vertically through the entire sample. Thus, we went on to develop TPA photolithography for creating axially complex, freeform 3D biochemical and biomechanical patterns and gradients in existing photoactive materials.

TPA has enabled the development of 3D fluorescence imaging,[14] 3D lithographic microfabrication,[15,16] and new approaches to 3D optical data storage.[15] Each of these applications takes advantage of the fact that, by tightly focusing an excitation beam, the region of TPA can be confined to a focal volume roughly half the excitation wavelength in dimension.[16] Any subsequent process, such as a photoinitiated or radical-based polymerization, is also localized to this small volume, assuming the timescale of radical diffusion to be large compared to the radical half life.[17] Thus, by specifying the location of the laser-beam focal point, regions of photoinduced conjugation can be precisely dictated.

In the present work, poly(ethylene glycol) (PEG)-diacrylate (PEGDA) hydrogels are used as model materials for the generation of internal 3D patterns. PEG-based materials have been studied extensively as tissue-engineering scaffolds[18] and are biocompatible and intrinsically resistant to protein adsorption and cell adhesion.[19] In addition, acrylate-terminated PEG macromers undergo rapid polymerization in the presence of photoinitiators that generate radicals when exposed to light.[18] Thus, PEGDA hydrogels are in themselves biological "blank slates" into which desired bioactivity can be tailored via light-based patterning.

To create 3D patterns using SPA photolithography, masks were first prepared by printing the lateral cross section of the desired pattern onto transparencies. A precursor solution containing appropriate photoinitiator and fluorescently labeled acryloyl (ACRL)-PEG-peptide or low-molecular-weight (MW) PEGDA was allowed to diffuse into a preswelled PEGDA hydrogel. The transparency mask was applied with the printed side in contact with the hydrogel surface, and the acrylate-derivatized moieties in the precursor solution were conjugated to specific regions within the hydrogel by applying UV light through the transparency mask.

Since the 600 MW PEGDA is diacrylate derivatized rather than monoacrylate derivatized (as is ACRL-PEG-peptide), immobilization of 600 MW PEGDA into the existing 6000 MW PEGDA hydrogel alters the local crosslinking density of the hydrogel (Fig. 1A).[20] Thus, the transport and mechanical

[*] Prof. J. L. West, Prof. M. S. Hahn,[+] J. S. Miller
Department of Bioengineering, Rice University
PO Box 1892, MS 142, Houston, TX 77251-1892 (USA)
E-mail: jwest@rice.edu

[+] Current address: Department of Chemical Engineering, 3122 Texas A&M University, College Station, TX 77843-3122, USA.

[**] The authors thank the NIH and NSF for funding. They also thank Kyriacos Athanasiou and Adrian Shieh for nanoindentation data, and Melissa McHale for help with the cell culture and with critical review of the manuscript.

ADVANCED MATERIALS

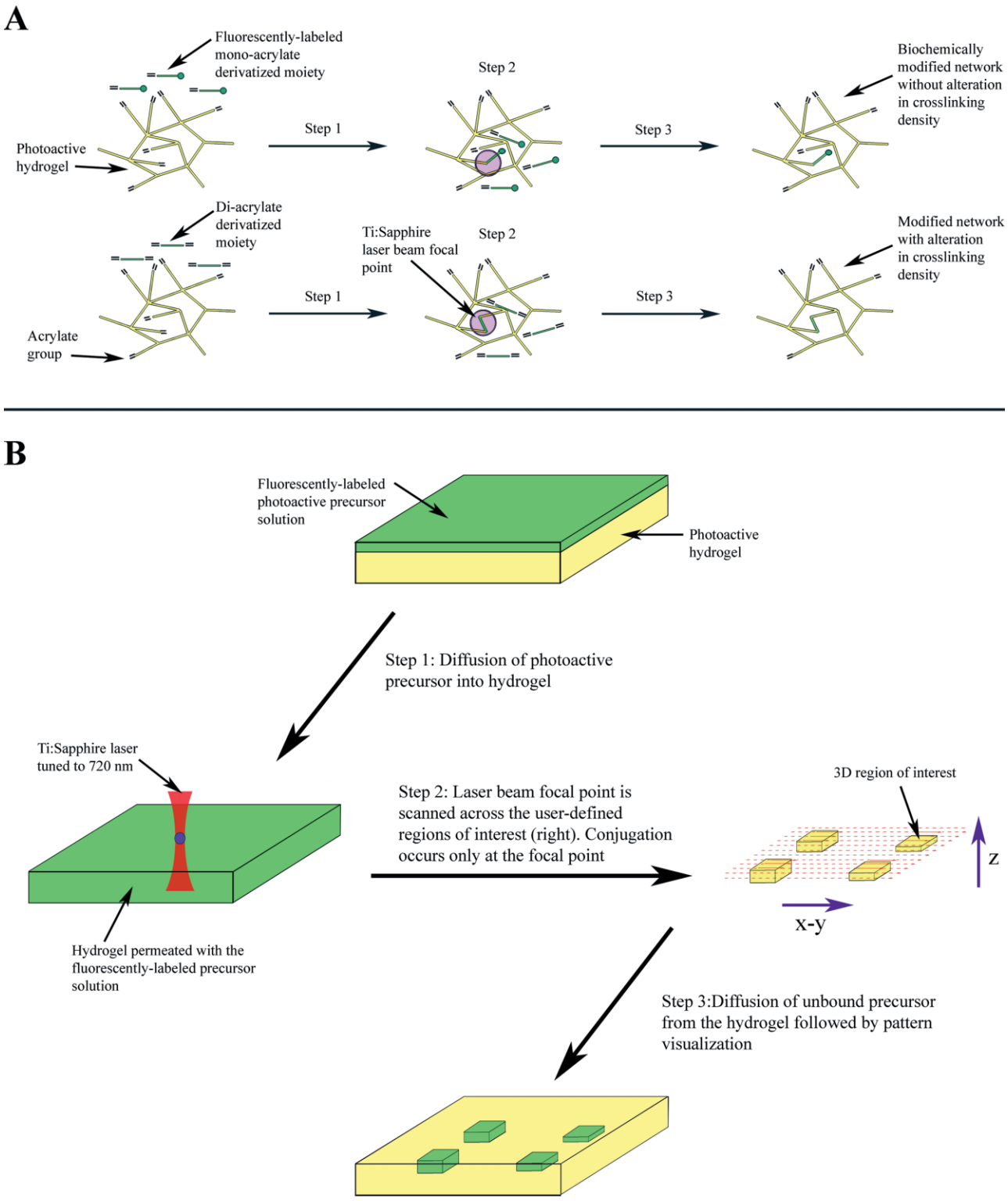

Figure 1. Schematics demonstrating photoinduced patterning of an existing poly(ethylene glycol) diacrylate (PEGDA) network at the microscale (A) and macroscale (B). The following description applies to both schematics. Step 1: Precursor solution containing the mono- or diacrylate derivatized moiety to be patterned is layered onto a base PEGDA hydrogel and allowed to diffuse into the hydrogel network. Step 2: A laser beam generated by a Ti:sapphire laser tuned to 720 nm is scanned across an *x*–*y* plane within the hydrogel, with the laser shutter being opened only in the user-specified regions of interest (ROIs) shown in the ROI template to the right of the hydrogel being patterned in (B). In TPA, conjugation of the molecule to be patterned to the hydrogel substrate occurs only at the laser focal point. The microscope stage is incremented axially and patterning is continued within the specific ROIs at this next *x*–*y* plane. This sequence of steps is repeated until the desired 3D patterns have been formed. Step 3: Unbound precursor is allowed to diffuse out of the hydrogel network.

properties of the hydrogel are regionally tailored. Figure 2A illustrates a differential interference contrast (DIC) image of a 6000 MW PEGDA hydrogel patterned with 600 MW PEGDA in stripes that extend throughout the gel thickness. The spatial alterations in hydrogel transport properties can be illustrated by examining the extent of diffusion of fluorescently labeled dextran (10 000 Da) into various regions of the patterned PEGDA hydrogel. As shown in Figure 2B, dextran was largely excluded from the 600 MW PEGDA patterned channels, but diffused freely through the unpatterned regions. To confirm the local change in hydrogel mechanical properties, a custom nanoindenter[21] fitted with a probe tip appropriate for the pattern dimensions and scaffold was used. The 6000 MW unpatterned regions had a compressive modulus of 3.3 <M+-> 0.5 kPa, roughly half the 7.3 <M+-> 1.2 kPa compressive modulus of the striped regions patterned with 600 MW PEGDA, $p = 0.0049$. These measured biomechanical properties, controlled at the microscale, are consistent with the previously reported MW-dependence of bulk PEG hydrogel compressive modulus.[20] Scaffold transport properties and pore size are critical parameters in tissue-engineering and drug-delivery applications.[20,22] In addition, cellular events are driven not only by biochemical cues, but also by the mechanical environment.[20,23] Thus, the ability to tailor material mechanical and transport properties at the cellular scale is highly desirable for a range of applications.

Although SPA photolithography permits rapid 3D patterning of photoactive substrates, the method is limited to the creation of patterns of uniform cross section that span the hydrogel thickness. To extend light-based patterning to the creation of freeform 3D patterns, the concept of TPA was used. A schematic of the general methodology for TPA photolithographic patterning of preformed PEGDA hydrogels is shown in Figure 1B. A precursor solution of fluorescently labeled ACRL-PEG-peptide or of low MW PEGDA containing a UV photoinitiator is allowed to diffuse into the PEGDA hydrogel, which is then positioned on the stage of a laser scanning microscope (LSM). Virtual masks, rather than conventional photolithographic masks, are created by drawing regions of interest (ROIs) onscreen using standard LSM software. These virtual masks are converted into irradiation instructions which dictate in 3D the pixel locations at which the laser shutter is opened. An irradiation cycle is then initiated in which the focal point of a mode-locked Ti:sapphire laser tuned to 720 nm

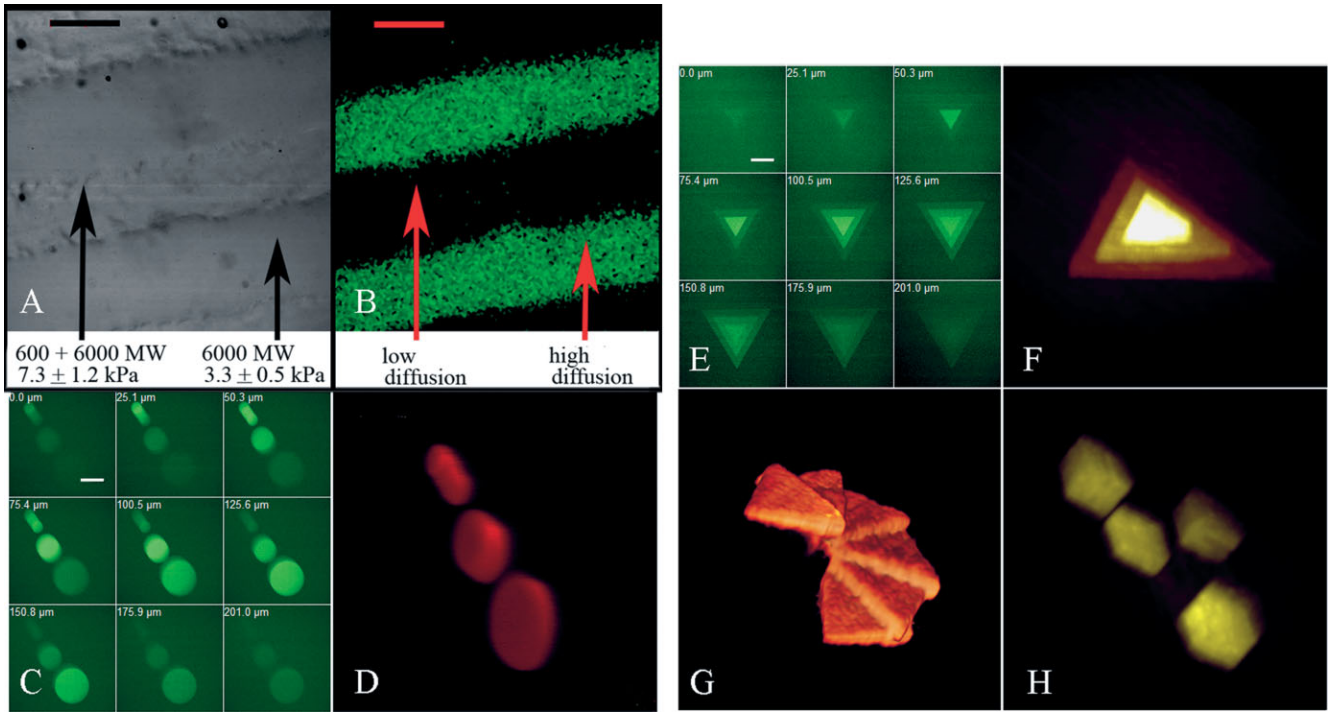

Figure 2. Patterns formed within existing hydrogel networks via SPA and TPA photolithographic patterning. A) DIC image of a 6000 MW PEGDA hydrogel 3D patterned with stripes of 600 MW PEGDA using SPA photolithography. B) The confocal image corresponding to (A) illustrating the exclusion of 10 000 Da fluorescently labeled dextran from the hydrogel regions patterned with 600 MW PEGDA. C) Confocal images at a series of *z*-planes of a PEGDA hydrogel patterned with fluorescently labeled ACRL-PEG-RGDS using TPA photolithography. Scale bar = 200 µm. D) 3D OsiriX rendering of the fluorescent image series in (C). E) Confocal images at a series of *z*-planes of a PEGDA hydrogel patterned with fluorescently labeled ACRL-PEG-RGDS using TPA photolithography. Exposure times were varied for each triangular structure, with the large base triangle and the intermediate triangle receiving 1/4 and 1/2 of the exposure time per micrometer squared, respectively, as the top triangle. Scale bar = 200 µm. F) 3D OsiriX rendering of the fluorescent images in (E), with each color reflecting a different fluorescence intensity and hence a different level of immobilized ACRL-PEG-RGDS. G) 3D OsiriX rendering based on a confocal image series of a hydrogel TPA photopatterned with a 3D spiral of fluorescently labeled ACRL-PEG-RGDS. H) 3D OsiriX rendering based on a confocal image series of a hydrogel TPA photopatterned with fluorescently labeled ACRL-PEG-RGDS in parallelograms of equal cross-sectional area (100 µm × 100 µm) but of varying heights.

ADVANCED MATERIALS

is scanned across the user-defined ROIs at the user-specified intensity and exposure times. By scanning only specific regions within each focal plane and then incrementing focal planes until a 3D pattern of desired dimensionality is achieved, spatially complex 3D patterns can be generated within existing hydrogel networks.

Figure 2C illustrates a sequence of *x*–*y* cross-sectional confocal images taken at a series of *z*-planes within a hydrogel patterned with fluorescently labeled ACRL-PEG-RGDS using TPA laser scanning lithography (LSL). Figure 2D shows the corresponding 3D volume rendering of this fluorescent image series. Note the lateral slant in each of the patterned cylinders. Axially punctuated or varying patterns such as these cannot be created using conventional SPA photolithography but can be generated readily using TPA LSL. An additional benefit of TPA LSL over SPA photolithography is that pre-existing patterns do not interfere with the fabrication of patterns in deeper hydrogel regions.[16] This results from the fact that not only is the difference in refractive index between patterned and unpatterned regions negligible, but also, the near-IR laser beam is not significantly absorbed by the PEGDA hydrogel, appropriately selected fluorophore, or photoinitiator.

By varying the irradiation exposure time or beam intensity during the TPA patterning cycle, the levels of immobilization can be spatially tailored, as demonstrated in Figure 2E and F. Conventional photolithographic methods cannot generate controlled 3D spatial gradients such as this. Surface biochemical gradients have been shown to have profound effects on the alignment, growth, and locomotion of a variety of cell types,[24–26] and spatial biochemical and biomechanical gradients are considered key to embryological morphogenesis. Thus, the ability to recapitulate complex gradient signals in three dimensions is important to numerous biotechnology applications. Additional 3D volume renderings generated from confocal images of PEGDA hydrogels patterned with fluorescently labeled ACRL-PEG-RGDS using TPA LSL are shown in Figure 2G and H to further illustrate the flexibility of this technique.

The TPA-generated patterns shown in Figure 2 each had the same dimensions as the specified ROIs within the resolution of the imaging system. Thus, pattern resolution for the present setup appears to be limited by the laser, with the diffusion of the photoinduced radicals away from the irradiated point having minimal effect on the resultant pattern fidelity. This result is likely due to the fact that we are patterning into an existing, relatively dense polymer network. This polymer network appears to cause the timescale of radical diffusion to be large compared to the radical half life.

To demonstrate the feasibility of using internally micropatterned materials to guide cell migration, we patterned rectangular channels of fluorescently labeled ACRL-PEG-RGDS into 1.5 mm thick collagenase-degradable hydrogels. The collagenase-sensitive peptide sequence used for the base hydrogel was GGPGQGILQGGK,[27] which was derivatized with mono-acrylated PEG at each terminus. Previous studies of cell migration into collagenase-degradable PEG hydrogels have shown that, in addition to sufficient levels of matrix metalloproteinase (MMP), appropriate levels of a peptide capable of promoting integrin-mediated cell adhesion, such as peptide RGDS, must be present for cell migration to occur.[28] Hence, by patterning ACRL-PEG-RGDS only in specific regions of the degradable hydrogel, we should be able to spatially confine cell migration to these regions.

Mean levels of bound RGDS within the patterned channels were determined to be ca. 1.7 <M+-> 0.3 μmol mL^{-1} by combining results from amino-acid analysis with known channel number and dimensions. Patterned hydrogels ($n = 3$) were placed into transwell inserts and HT-1080 fibrosarcoma cells, a commonly used cell type in migration studies,[29] were seeded on top of the gels. After four weeks in culture, cells were labeled with Orange Cell Tracker and 4′,6-diamidino-2-phenylindole (DAPI), and migration was assessed using confocal microscopy. Figure 3A illustrates a representative *x*–*y* cross-sectional confocal image taken within an RGDS-patterned collagenase-degradable PEG hydrogel. Note that migrating cells are isolated to the fluorescently labeled RGDS channel and are not found in the surrounding unpatterned regions. A side view of the RGDS channel clearly illustrates the extent of cellular migration into the patterned hydrogel (Fig. 3B).

Cell migration is an essential component of tissue development and homeostasis, embryological morphogenesis, inflammation, tissue repair, angiogenesis, and immune surveillance.[30] Cell migration also plays a key role in determining

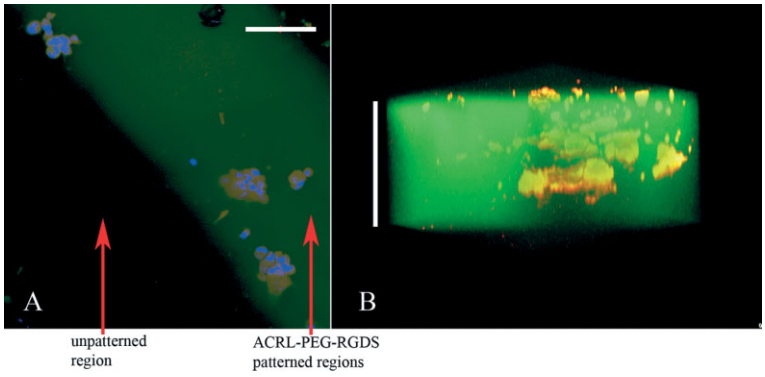

Figure 3. Cell migration confined to the ACRL-PEG-RGDS patterned channels of collagenase-degradable PEG hydrogels. A) Confocal cross-sectional image taken ca. 50 μm into the hydrogel, demonstrating the confinement of migrating HT-1080 cells (cytoplasm: orange; nuclei: blue) to the fluorescently labeled ACRL-PEG-RGDS patterned channels (green). Scale bar = 100 μm. B) Side view of a 3D OsiriX volume rendering of a confocal image series (*z*-stack) of an ACRL-PEG-RGDS (green) patterned, collagenase-degradable hydrogel into which HT-1080 cell clusters (orange) had migrated. Scale bar = 550 μm. The apparent unevenness in RGDS intensity observed in (B) is primarily due not to actual unevenness in RGDS patterning intensity but to imaging artifacts.

the structure and growth rate of bioartificial tissues.[31] Thus, significant attention has recently focused on developing biomimetic materials capable of promoting migration. As such, the ability of the patterning modality presented herein to guide cell migration within scaffolds represents a substantial advance. Possible extensions include the creation of microvascular networks in 3D tissue-engineered scaffolds via controlled endothelial cell migration.

In summary, we have presented a new paradigm for the fabrication of internally complex materials via controlled 3D patterning within existing photoactive scaffolds rather than via conventional layer-by-layer techniques. This paradigm has been validated using SPA and TPA photolithography to internally immobilize mono- and diacrylate-derivatized moieties into preformed PEGDA hydrogels. These same methodologies can be readily applied to any optically transparent, photoactive substrate that permits diffusion of the molecule to be patterned. In addition, this patterning methodology can potentially be extended to the creation of complex 3D structures on surfaces rather than within existing networks; however, the effects of diffusion on patterning outcome would likely become significant in these situations. SPA photolithography allows for the facile and inexpensive patterning of material biochemical and biomechanical properties when axial control is not required. TPA LSL, in contrast, permits axial as well as lateral control over patterning exposure time and pattern feature size, resulting in a versatile method for the creation of freeform biochemical and biomechanical patterns and complex 3D gradients within existing materials. As demonstrated herein, internally complex materials generated under this paradigm can be used to guide cell migration, and thus this approach represents a powerful avenue for the exploration of a range of fundamental questions in biotechnology.

Experimental

Polymer Synthesis: PEGDA 6000 MW, PEGDA 3400 MW, and Alexa Fluor 488-labeled ACRL-PEG-RGDS were synthesized as previously described [32]. The collagenase-sensitive peptide sequence GGPQGILGQGGK was prepared using Fmoc solid-phase peptide synthesis (Applied Biosystems), cleaved from the resin, then conjugated to two ACRL-PEG-NHS chains, and purified by dialysis as previously described [28].

Patterning Method: A solution of 10 % (w/v) PEGDA (ACRL-PEG-peptide-PEG-ACRL) in HEPES buffered saline (HBS, pH 7.4) was prepared. 10 $\mu L\,mL^{-1}$ of 300 $mg\,mL^{-1}$ 2,2-dimethoxy-2-phenylacetophenone (DMAP) in *N*-vinylpyrrolidone (NVP) was added to solution, which was then polymerized between two clamped glass plates separated by 0.5 mm (or 1.5 mm) spacers via exposure to a 10 $mW\,cm^{-2}$, 365 nm UV lamp for 1 min (or 2 min). The upper glass plate was removed and the gel allowed to swell for 1 h in sterile HBS. A precursor solution containing either 30 $\mu mol\,mL^{-1}$ ACRL-PEG-RGDS or 30 % (w/v) 600 MW PEGDA in HBS supplemented with 1 % (v/v) 300 $mg\,mL^{-1}$ DMAP in NVP was applied to the gel surface and allowed to diffuse into the gel for 3 h at 37 °C.

SPA Photolithography: The desired patterns were prepared using Photoshop and printed onto transparencies using a laser jet printer (LaserWriter 16/600 PS). Excess precursor solution was aspirated off the base PEGDA hydrogel, and the patterned transparency was overlaid with the printed side in contact with the hydrogel surface. The upper glass plate was replaced, clamped, and UV light applied through the transparency mask for 1–2 min, depending on the desired level of precursor immobilization. The gel was immersed in HBS and unbound precursor was allowed to diffuse out of the gel.

TPA LSL: The base hydrogel into which precursor solution had diffused was positioned at the focal plane of a 10 × Plan-Apochromat objective (numerical aperture *NA* 0.45) attached to a LSM 510 META confocal microscope (Zeiss). Virtual masks were drawn using the ROI functionality of the LSM software. All TPA LSL patterning, excluding gradient patterning, was carried out using an irradiation cycle in which a Ti:sapphire laser tuned to 720 nm was scanned in the *x*–*y* dimension across the specified ROIs at 225 $mW\,\mu m^{-2}$ and 120 $\mu s\,\mu m^{-2}$. The *z*-limiting functionality of the ROIs allowed the final and initial planes of each ROI in a group to be separately defined and controlled. Spatial gradients of immobilized ACRL-PEG-RGDS were formed by altering the exposure time used in various ROIs. The gel was immersed in HBS and unbound ACRL-PEG-RGDS was allowed to diffuse out of the gel. Successful patterning of the fluorescently labeled peptide was confirmed by using confocal microscopy.

Analysis of Transport and Mechanical Property Patterning: A custom nanoindenter [21] equipped with a probe tip of diameter $D = 76.2$ μm was used to measure the mechanical properties of a 0.5 mm thick 6000 MW hydrogel into which 200 μm wide channels of 600 MW PEGDA had been patterned using SPA photolithography. A force $F = 8$ μN was exerted and the resulting displacement, d, was measured in triplicate for both patterned and unpatterned regions and used to calculate the modulus of the material according to the following equation, which assumes a perfectly linearly elastic material

$$E = \frac{F(1-\nu^2)}{Dd} \quad (1)$$

where E is the compressive modulus and ν is the material Poisson's ratio, assumed to be 0.4 [33]. The statistical significance of the difference in the measured mechanical properties between patterned and unpatterned regions was determined using a two-tailed student *t*-test, $p < 0.05$. To demonstrate alterations in hydrogel transport properties introduced via patterning with diacrylate derivatized moieties, the hydrogel was immersed in a 1 $mg\,mL^{-1}$ solution of fluorescently labeled 10 000 Da dextran (Invitrogen) dissolved in HBS overnight at room temperature. Spatial variations in the diffusion of the dextran into the hydrogel were examined using confocal microscopy.

Cell-Migration Studies: HT-1080 human fibrosarcoma cells (American Type Culture Collection (ATCC)) were maintained in MEM (ATCC) supplemented with 10 % fetal bovine serum (Sigma) and 10 $\mu g\,mL^{-1}$ Ciprofloxacin (Sigma) at 37 °C/5 % CO_2. ACRL-PEG-GGPQGILGQGGK-PEG-ACRL hydrogels were patterned with rectangles of Alexa Fluor 488-labeled ACRL-PEG-RGDS, as described above. Patterned hydrogels ($n = 3$) were placed into transwell inserts (BD Biosciences, 8 μm pores) and HT-1080 cells (passage 4–7) were seeded on top of the gels. Media was changed every three days and after four weeks cells which had migrated into the hydrogels were labeled with Cell Tracker Orange (Invitrogen), fixed briefly in paraformaldehyde, and stained with DAPI. The extent of HT-1080 migration into the hydrogels was confirmed using confocal microscopy. The mean RGDS concentration in the patterned channels of each collagenase degradable hydrogel was calculated by dividing the total micromoles of RGDS per milliliter of hydrogel measured by amino-acid analysis (AAA Service Lab) by the fraction of the hydrogel volume patterned with ACRL-PEG-RGDS.

Received: March 27, 2006
Published online: September 15, 2006

[1] C. S. Chen, X. Y. Jiang, G. M. Whitesides, *MRS Bull.* **2005**, *30*, 194.
[2] R. McBeath, D. M. Pirone, C. M. Nelson, K. Bhadriraju, C. S. Chen, *Dev. Cell* **2004**, *6*, 483.
[3] V. A. Liu, S. N. Bhatia, *Biomed. Microdevices* **2002**, *4*, 257.

[4] J. Z. Hilt, A. K. Gupta, R. Bashir, N. A. Peppas, *Biomed. Microdevices* **2003**, *5*, 77.
[5] R. Fernandes, L.-Q. Wu, T. Chen, H. Yi, G. W. Rubloff, R. Ghodssi, W. E. Bentley, G. F. Payne, *Langmuir* **2003**, *19*, 4058.
[6] V. Mironov, T. Boland, T. Trusk, G. Forgacs, R. Markwald, *Trends Biotechnol.* **2003**, *21*, 157.
[7] W. Tan, T. Desai, *Biomed. Microdevices* **2003**, *5*, 235.
[8] K. Y. Suh, J. Seong, A. Khademhosseini, P. E. Laibinis, R. Langer, *Biomaterials* **2004**, *25*, 557.
[9] J. Tien, C. M. Nelson, C. S. Chen, *Proc. Natl. Acad. Sci. USA* **2002**, *99*, 1758.
[10] R. S. Kane, S. Takayama, E. Ostuni, D. E. Ingber, G. M. Whitesides, *Biomaterials* **1999**, *20*, 2363.
[11] Y. Luo, M. Shoichet, *Nat. Mater.* **2004**, *3*, 249.
[12] J. B. Hutchison, P. F. Stark, C. J. Hawker, K. S. Anseth, *Chem. Mater.* **2005**, *17*, 4789.
[13] M. Borkenhagen, J.-F. Clemence, H. Sigrist, P. Aebischer, *J. Biomed. Mater. Res.* **1998**, *40*, 392.
[14] W. Denk, J. H. Strickler, W. W. Webb, *Science* **1990**, *248*, 73.
[15] B. H. Cumpston, S. P. Ananthavel, S. Barlow, D. L. Dyer, J. E. Ehrlich, L. L. Erskine, A. A. Heikal, S. M. Kuebler, I.-Y. S. Lee, D. McCord-Maughon, J. Qin, H. Röckel, M. Rumi, X.-L. Wu, S. R. Marder, J. W. Perry, *Nature* **1999**, *6722*, 51.
[16] S. Maruo, O. Nakamura, S. Kawata, *Opt. Lett.* **1997**, *22*, 132.
[17] S. Kuebler, K. Braun, W. Zhou, J. K. Cammack, T. Yu, C. K. Ober, S. R. Marder, J. W. Perry, *J. Photochem. Photobiol. A* **2003**, *158*, 163.
[18] K. T. Nguyen, J. L. West, *Biomaterials* **2002**, *23*, 4307.
[19] W. R. Gombotz, G. H. Wang, T. A. Horbett, A. S. Hoffman, *J. Biomed. Mater. Res.* **1991**, *25*, 1547.
[20] S. J. Bryant, T. T. Chowdhury, D. A. Lee, D. L. Bader, K. S. Anseth, *Ann. Biomed. Eng.* **2004**, *32*, 407.
[21] E. Koay, A. Shieh, K. Athanasiou, *J. Biomech. Eng.* **2003**, *125*, 334.
[22] A. W. Watkins, K. S. Anseth, *Macromolecules* **2005**, *38*, 1326.
[23] D. S. Gray, J. Tien, C. S. Chen, *J. Biomed. Mater. Res. Part A* **2003**, *66*, 605.
[24] Y. Ito, M. Hayashi, Y. Imanishi, *J. Biomater. Sci. Polym. Ed.* **2001**, *12*, 367.
[25] S. K. Dertinger, X. Jiang, Z. Li, V. N. Murthy, G. M. Whitesides, *Proc. Natl. Acad. Sci. USA* **2002**, *99*, 12 542.
[26] G. Chen, Y. Ito, *Biomaterials* **2001**, *22*, 2453.
[27] *Matrix Metalloproteinases* (Eds: W. Parks, R. Mecham), Academic, San Diego, CA **1998**.
[28] A. S. Gobin, J. L. West, *FASEB J.* **2002**, *16*, 751.
[29] Z. N. Demou, L. V. McIntire, *Cancer Res.* **2002**, *62*, 5301.
[30] P. Friedl, E.-B. Brocker, *Cell. Mol. Life Sci.* **2000**, *57*, 41.
[31] R. Langer, J. Vacanti, *Tissue Engineering Science* **1993**, *260*, 920.
[32] M. S. Hahn, J. S. Miller, J. L. West, *Adv. Mater.*, in press.
[33] J. W. Harding, I. N. Sneddon, *Proc. Cambridge Philos. Soc.* **1945**, *41*, 16.

